energies

MDPI

Article

Method of Geomechanical Parameter Determination and Volumetric Fracturing Factor Simulation under Highly Stochastic Geologic Conditions

Dongmei Ding [1], Yongbin Wu [2,*], Xueling Xia [1], Weina Li [1], Jipeng Zhang [3] and Pengcheng Liu [3]

[1] Beijing Sunshine Geo-Tech Co., Ltd., Beijing 100192, China
[2] Research Institute of Petroleum Exploration and Development, PetroChina, Beijing 100083, China
[3] School of Energy Resources, China University of Geosciences, Beijing 100083, China
* Correspondence: wuyongbin@petrochina.com.cn

Abstract: In order to accurately predict geomechanical parameters of oil-bearing reservoirs and influencing factors of volumetric fracturing, a new method of geomechanical parameter prediction combining seismic inversion, well logging interpretation and production data is proposed in this paper. Herein, we present a structure model, petrophysical model and geomechanical model. Moreover, a three-dimensional geomechanical model of a typical reservoir was established and corrected using history matching. On this basis, a typical well model was established, 11 influencing factors of volume fracturing including formation parameters and fracturing parameters were analyzed and their impact were ranked, and the oil recovery rate and the accumulated oil production before and after optimal fracturing were compared. The results show that with respect to formation parameters, reservoir thickness is the main influencing factor; interlayer thickness and stress difference are the secondary influencing factors; and formation permeability, Young's modulus and Poisson's ratio are the weak influencing factors. For a pilot well of a typical reservoir, the optimized fracture increased production by 7 tons/day relative to traditional fracturing. After one year of production, the method increased production by 4 tons/day relative to traditional fracturing, showing great potential in similar oil reservoirs.

Keywords: volumetric fracturing; low-permeability reservoir; geomechanical parameters; oil recovery

Citation: Ding, D.; Wu, Y.; Xia, X.; Li, W.; Zhang, J.; Liu, P. Method of Geomechanical Parameter Determination and Volumetric Fracturing Factor Simulation under Highly Stochastic Geologic Conditions. *Energies* **2023**, *16*, 312. https://doi.org/10.3390/en16010312

Academic Editor: Reza Rezaee

Received: 26 November 2022
Revised: 23 December 2022
Accepted: 24 December 2022
Published: 27 December 2022

1. Introduction

Volumetric fracturing has become the primary stimulation method for oil recovery from low-to-tight permeability reservoirs in recent years. For reservoirs with extensive existing wells, the geologic parameters are relatively deterministic, and the operation parameters of volumetric fracturing can be obtained based on existing geomechanical information. In contrast, for new reservoirs with few or no existing wells, the spatial distribution of geologic and geomechanical parameters is highly stochastic, and drilling and volumetric fracturing are highly risky [1–4]. According to PetroChina statistics, the past ratio of economic production in newly developed tight oil reservoirs with volumetric fractured wells is less than 40%. It is increasingly realized that a new method should be proposed on the basis of the traditional method of geomechanical parameter determination based purely on well logging data to massively improve the success ratio of volumetric fracturing.

Traditionally, geomechanical parameters were obtained from the correlation functions of the geomechanical parameters with logging parameters, such as Young's modulus and Poisson ratio, with gamma and acoustic logging data. This method has detrimental disadvantages, as logging data are only a reflection of the rock parameters in the wellbore or the well vicinity region. Whereas volumetric fracture development is considerably affected by the rock lithology, petrophysical parameters induce heterogeneous geomechanical parameters in the region far from the wellbore [5–8].

Under highly uncertain geologic conditions or in reservoirs with few or no wells, the petrophysical properties interpreted from well logging data are in poor agreement with the real spatial distribution of these parameters. In order to improve the success ratio of geomechanical parameter prediction, researchers have proposed various methods that have been applied in the field with both success and failure. It has been found that the accurate prediction of geomechanical parameters is a prerequisite for successful volumetric fracturing operation. The use of an ensemble long short-term memory (EnLSTM) network in well log generation [9] is one such method for predicting geomechanical parameters based on well logging interpretation. Researchers trained an interpretation model based on an available data set and combined an ensemble neural network and a cascaded LSTM network to improve the model accuracy in interpretation. In order to deal with the issues of overconvergence and disturbance compensation, two methods were applied, which improved the accuracy in interpreting the geomechanical properties from well logging data.

Geomechanical properties can also be obtained from drilling data [4,10,11]. A cost-effective technology was proposed that uses commonly available drilling data to deduce the geomechanical properties of rock without the need for downhole logging operations and interpretation. In order to accurately calculate the friction parameters of the wellbore and the downhole weight on a bit, a new wellbore friction model was built and validated using field data. Based on this, the formation lithology constants for different rock types were used to assist in calculating the geomechanical properties of reservoir formations, including confined compressive strength (CCS), unconfined compressive strength (UCS), Young's modulus, permeability, porosity and Poisson's ratio.

Artificial intelligence neural networks, data mining, machine learning techniques and deep learning have also been introduced to estimate dynamic geomechanical properties, including Poisson's ratio, Young's modulus and Lamé parameters [12–17]. Furthermore, the application of core and log data is also used to predict rock mechanics. For example, porosity can be employed as a geomechanical index to enable the estimation of rock mechanic material properties using general and field-specific correlations [18].

Sequence stratigraphy and geomechanics also have some correlations, as many geological properties affect geomechanical properties and, ultimately, reservoir operations and performance [19]. Petroelastic and geomechanical classification of lithologic facies also have correlations to some extent, representing a new research frontier [20]; through the analysis of rock facies and rock properties, the correlations between petroelastic and geomechanical properties can be determined.

Principal stresses, including the vertical, maximum horizontal and minimum horizontal stresses, and elastic moduli related to rock brittleness, such as Young's modulus and Poisson's ratio, can also be estimated from wide-angle, wide-azimuth 3D seismic data, which were used to optimize the placement and direction of horizontal wells and hydraulic fracture stimulations [21].

The combination of well logs and seismic reflection data to predict geomechanical data is a new trend [22]. Researchers investigated the wireline log data of four wells and regional seismic reflection data and establish a workflow for accurate estimation of geomechanical parameters; this process was validated by field volumetric fracturing parameter optimization and successful implementations. Investigators found that the precise estimation of reservoir geomechanical parameters using this method can reduce risk and provide benefits throughout the lifespan of an oil and gas field.

In this work, we propose a new geomechanical parameter prediction method coupling both seismic reversion and well logging interpretation data, based on which a typical well model was built, the influence factors of volumetric fracturing were simulated and their impacts were determined. Finally, a typical pilot test well was designed, fracturing parameters were optimized and the production before and after fracturing optimization was predicted and compared, which validated the feasibility and accuracy of the methodology proposed in this study.

2. Geomechanical Property Modeling Method Coupling Logging and Seismic Reflection Data

At present, commonly used modeling methods include deterministic modeling, stochastic modeling, etc. For the parameters that can be determined, the deterministic modeling method is preferred. For parameters with many influencing factors, the method of combining deterministic modeling with stochastic modeling is considered. Especially when random modeling is used, seismic reflection data are used to constrain the well so as to reduce the uncertainty of the model and improve the accuracy of the 3D geological model. The target geological model presented in this study is set up mainly adopting the method of combining deterministic modeling and stochastic modeling, making full use of the characteristics of logging data with high vertical resolution, seismic data and the second variable involved in the geological model of simulation calculation. In areas with multiple wells, deterministic modeling is performed on the basis of well data, with reference to earthquake information. In areas without wells, seismic information is mainly used for simulation operation, not only making full use of well data but also overcoming the difficulty of controlling the structure and reservoir due to the low drilling density, enhancing the reliability of the established geological model. Moreover, for well sections with information about already fractured wells, history matching is used to further calibrate the geomechanical parameters that affect the volumetric fracturing result and the production performance.

The overall workflow used to extract a geomechanical model from existing geologic, seismic, fracturing and production information is shown in Figure 1. The major difference from traditional modeling is that the seismic reflection data are used to constrain the determined well logging interpretation and stochastic lithofacies; structure and petrophysical modeling are used to ensure reasonable spatial distribution of the structure, lithofacies and petrophysical properties; and the fracturing and production dynamic data are used to further calibrate the model properties mentioned above. Moreover, the fracturing and production dynamic data are used in combination with the geomechanical functions to extract the 3D geomechanical model.

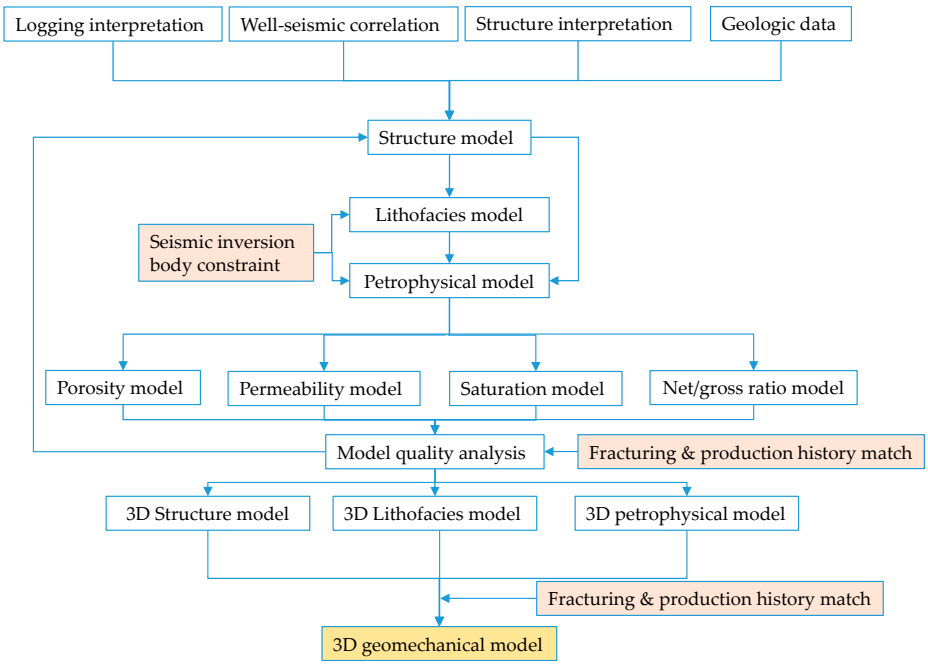

Figure 1. The overall workflow used to extract geomechanical model.

The specific method and steps are as follows:

(1) Establish a high-precision 3D structure model

Based on the fault data, layer data and single-well geological stratification data provided by seismic interpretation, in combination with reservoir development characteristics, formation thickness distribution variation under a tectonic background and the contact relationship between each sublayer, reasonable mesh division and modeling methods are adopted to establish a high-precision 3D structure model. Then, 3D seismic data and drilling data are used to check and control the structural model.

(2) Establish a 3D petrophysical model characterizing lithofacies and reservoir parameters

Figure 2 shows the workflow of a fine 3D petrophysical model. Because it is difficult to describe the spatial distribution of the reservoir parameters with interwell interpolation alone, the logging interpretation results of reservoir sandstone, tight sandstone and mudstone are used in single-well lithoface division and inversion body correlation analysis. According to the analysis result, the inversion body is adopted as a constraint control to improve the lithoface model. Under the constraint of the lithoface model, taking porosity, permeability and oil saturation of logging interpretation as input data, in combination with the seismic inversion body of reservoir parameters, using geostatistics and the lithoface-controlled random simulation method, fine reservoir parameter models are established.

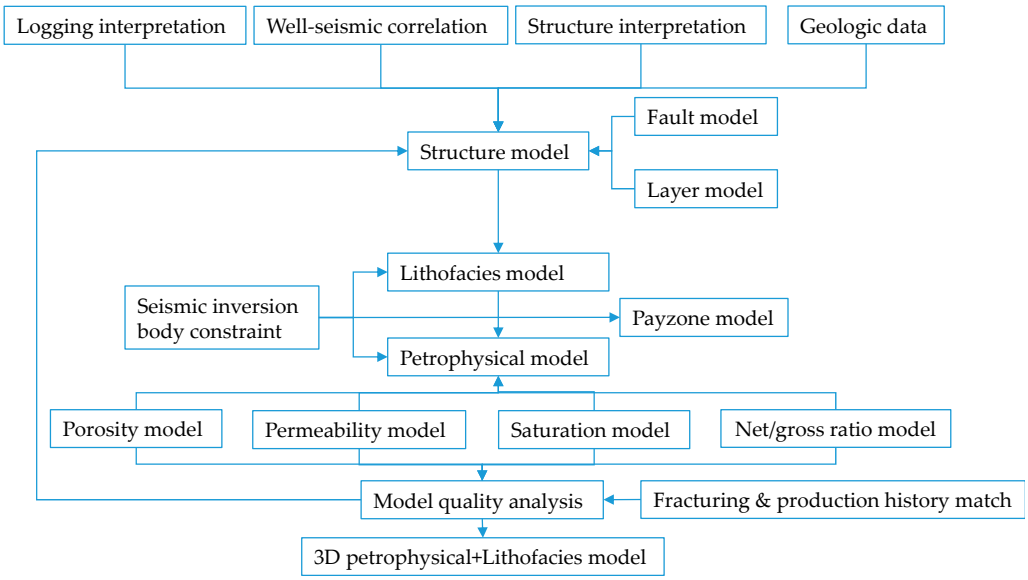

Figure 2. Workflow of the fine 3D petrophysical model.

(3) Establish a 3D geological model characterizing geomechanical parameters

Figure 3 shows the workflow of the fine 3D geomechanical model. The 3D geomechanical model has multiple properties, including overburden pressure, payzone pore pressure, maximum and minimum horizontal principal stress, uniaxial compressive strength, Young's modulus, Poisson's ratio and brittleness index. A modified method was adopted in building a geomechanical model distinct from the traditional single-well geomechanical model. It should be noted that the seismic inversion body-constrained structure model and lithoface model were used for spatial characterization of the geomechanical model, and history matching using existing fracturing and production dynamic data was also necessary for further calibration of the geomechanical model.

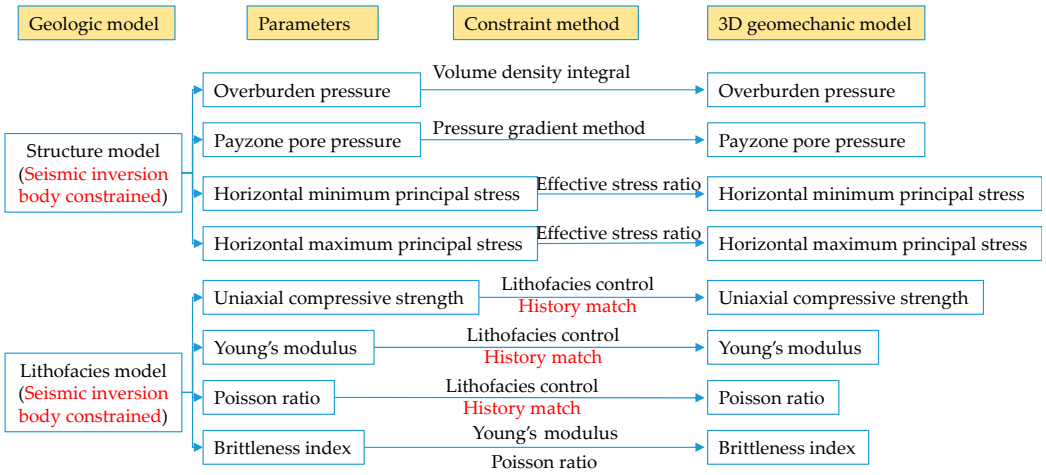

Figure 3. Workflow of the fine 3D geomechanical model.

3. Geomechanical Property Modeling for a Typical Reservoir

3.1. Overburden Pressure

Figure 4 shows the overburden pressure modeling workflow. As shown in Figure 4a–c, the overburden pressure is density-integral. According to the density curve from the ground to the bottom of the well fitted by a single well, density modeling is carried out in combination with the 3D geological model grid to obtain the density body from the ground to the target layer in the whole region; then, the three-dimensional overburden pressure body is obtained by density integral. The pressure distribution range of overlying strata in target formation is 32 MPa–40 MPa. The parameter maps and cross-section maps show that the pressure of the overlying strata is mainly affected by the buried depth of strata and increases gradually from north to south.

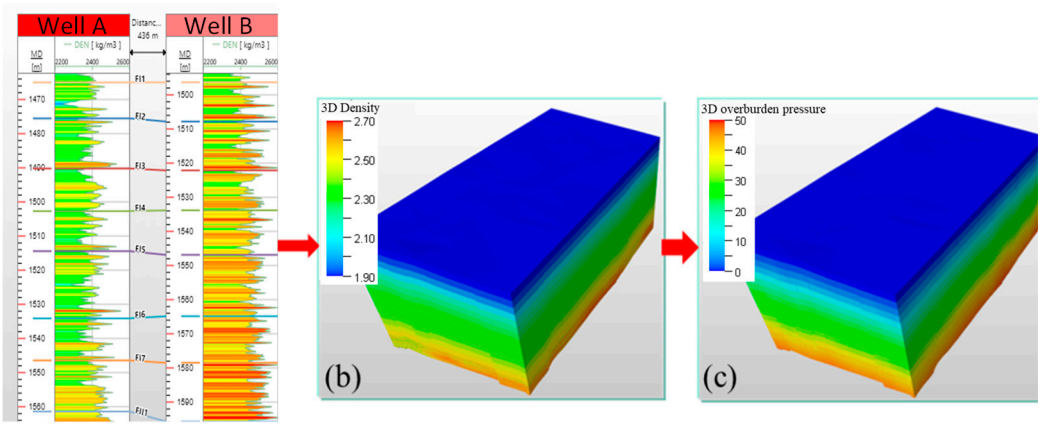

(**a**)

Figure 4. Overburden pressure modeling workflow. (**a**) Single-well density curve; (**b**) 3D density model; (**c**) 3D overburden pressure model.

3.2. Three-Dimensional Pore Pressure

The basic principle of pore pressure prediction is under-compaction theory. Under normal circumstances, the stratum is gradually compacted and diagenetic under the pressure of the overlying stratum. The fluid in the pores of the stratum is gradually discharged during the compaction process, and the pressure of the overlying stratum is mainly borne by the rock skeleton. The pore fluid only carries hydrostatic pressure in the pores, and the formation porosity decreases exponentially with increasing depth.

If depth is linear and porosity is logarithmic, the depth–porosity curve is a straight line. Because the sonic velocity of the formation is linear to porosity, the velocity curve or sonic time difference curve is also a straight line, representing normal compaction.

When the sedimentary stratum is a large set of mudstone or sand–mud mixed sedimentation, the stratum permeability is very low. During the compaction diagenesis process, the stratum fluid (mainly water) cannot be discharged, and the pore fluid not only bears hydrostatic pressure but also a part of the overlying stratum pressure, so high pressure occurs. Because the pore fluid carries part of the pressure of the overlying strata, the pressure of the rock skeleton is reduced and therefore cannot be fully compacted, retaining high pore pressure, which is often referred to as "under-compacted".

Pressure anomalies due to under-compaction preserve higher porosity and lower sonic or seismic velocities. This characteristic of the under-pressed field stratum is the theoretical basis of pressure prediction, that is, the pore pressure can be predicted by using the low-velocity anomaly of velocity. Therefore, the Eaton method is used to forecast the pore pressure, as expressed by the following equation [23].

$$P_{\mathrm{p}} = S_{\mathrm{v}} - (S_{\mathrm{v}} - P_{\mathrm{h}})\left(\frac{t_{\mathrm{n}}}{t_{\mathrm{o}}}\right)^{N} \quad (1)$$

where P_{p} refers to the predicted payzone pore pressure (MPa), S_{v} is the overburden pore pressure (MPa), P_{h} is the hydrostatic pressure (MPa); t_n is the reciprocal of seismic velocity under normal compaction (μs/ft); t_{o} is the reciprocal of measured seismic velocity (μs/ft) and N is the Eaton index.

Figure 5 shows the cross-section map of the pore pressure coefficient in the N–S direction. As shown in Figure 5, due to the influence of stratum burial depth, the pore pressure of the southern formation is higher, but the change in pore pressure coefficient is minimal, ranging from 1.25 to 1.50 on the whole, with an average of approximately 1.30. The pore pressure of the target stratum of the target formation in this study is distributed in the range of 18–26 MPa. As can be seen from the cross-section map of pore pressure in the whole area, there is little difference in the values of sand and mudstone, and the main distribution range is 20–23 MPa.

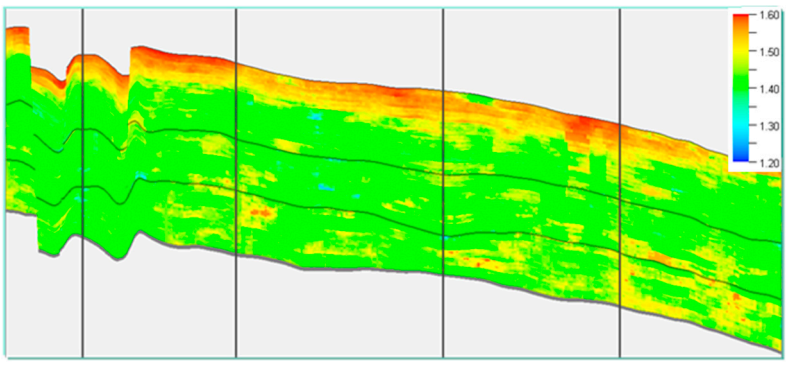

Figure 5. Cross-section map of the pore pressure coefficient in the N–S direction.

3.3. Three-Dimensional Horizontal Principal Stress

Three-dimensional horizontal principal stress is calculated by the combined spring model. Conventional logging and drilling mud data are absent from imaging logging data in the process of determining the structural coefficient. Therefore, determination of the structural coefficient refers to the rock failure test of only one well in this area and that of the adjacent area, taking $\varepsilon_{\mathrm{x}} = 0.0001$, $\varepsilon_{\mathrm{y}} = 0.0005$ and Biot coefficient = 0.8 to calculate

the minimum and maximum horizontal principal stress in the whole area. The following equations are used to calculate the maximum and minimum horizontal principal stress [24].

$$S_{\text{hmin}} = \frac{v}{1-v}S_{\text{v}} + \frac{1-2v}{1-v}\alpha P_{\text{p}} + \frac{E}{1-v^2}\varepsilon_{\text{x}} + \frac{vE}{1-v^2}\varepsilon_{\text{y}} \quad (2)$$

$$S_{\text{hmax}} = \frac{v}{1-v}S_{\text{v}} + \frac{1-2v}{1-v}\alpha P_{\text{p}} + \frac{E}{1-v^2}\varepsilon_{\text{y}} + \frac{vE}{1-v^2}\varepsilon_{\text{x}} \quad (3)$$

where S_{hmin} is the horizontal minimum principal stress (MPa), S_{hmax} is the horizontal maximum principal stress (MPa), v is the Poisson ratio (f), E is the Young's modulus (MPa), α is the Biot coefficient (f), S_{v} is the overburden pressure (MPa) and P_{p} is the pore pressure (MPa).

Figure 6 shows the cross-section map of minimum horizontal principal stress in the N–S direction. As shown in Figure 6, the minimum horizontal principal stress increases gradually from north to south and from top to bottom, with a distribution range of 25–32 MPa and an average of 27.6 MPa. The plane changes gradually, which is conducive to the uniform propagation of fractures.

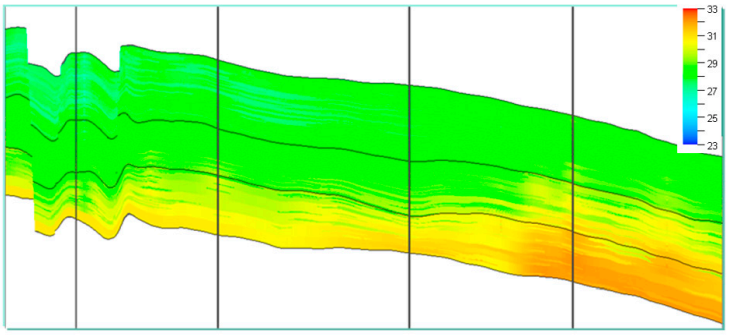

Figure 6. Cross-section map of minimum horizontal principal stress in the N–S direction.

3.4. Three-Dimensional Horizontal Stress Difference

Figure 7 shows the cross-section map of horizontal principal stress difference in the N–S direction. As shown in Figure 7, the horizontal stress difference can be calculated using the maximum horizontal principal stress and the minimum horizontal principal stress. The horizontal stress difference in the area is between 2 and 10 MPa, with an average of 5.7 MPa. The distribution characteristics of horizontal stress difference were statistically analyzed according to lithology categories; the mudstone horizontal stress difference is slightly lower than sandstone horizontal stress difference because the sand maximum horizontal principal stress is close to that of mudstone, whereas the minimum horizontal principal stress of sandstone is slightly lower than that of mudstone. The main distribution range of horizontal stress difference is conducive to the formation of a complex fracture network.

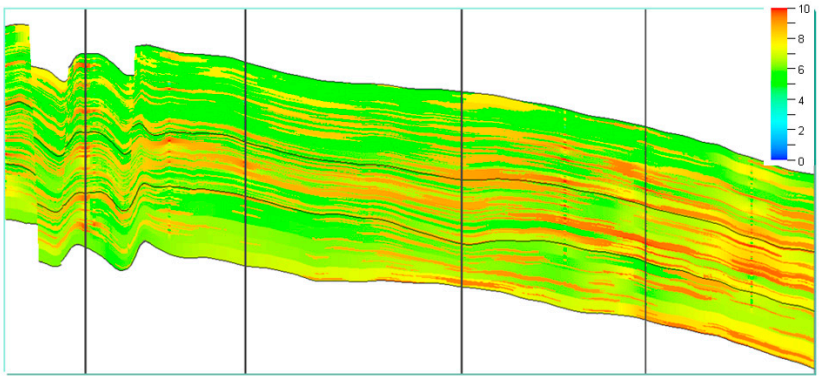

Figure 7. Cross-section map of horizontal principal stress difference in the N–S direction.

3.5. Three-Dimensional Rock Geomechanical Parameters

Lithology directly affects the uniaxial compressive strength, Young's modulus, Poisson's ratio and other mechanical properties, so the face-controlled modeling method is used to establish a three-dimensional rock mechanical parameter model. In addition, the brittleness index is the basis for the formation of fracture networks in tight reservoirs during fracturing. In this study, we also calculated the formation brittleness in the study area. The calculation method of normalized Young's modulus and Poisson's ratio was adopted (Rickman R, 2008). The brittleness of rock is expressed as the relationship between stress and strain in rock mechanics. Poisson's ratio is used to characterize the relationship between the transverse strain caused by uniformly distributed longitudinal stress and the corresponding longitudinal strain. Young's modulus is a parameter describing the relationship between longitudinal stress and longitudinal strain caused by longitudinal stress. Therefore, the Poisson's ratio and Young's modulus of rock elastic parameters can be used to calculate the brittleness index. The equation of calculation is as follows [25].

Figure 8 shows the cross-section map of Young's modulus in the N–S direction. Figure 9 shows the cross-section map of Poisson's ratio in the N–S direction. Figure 10 shows the cross-section map of the brittleness index in the N–S direction. Analysis of the calculated mechanical parameter model results shows that the distribution range of Young's modulus, Poisson's ratio and the brittleness index in the target formation is 15–27 GPa, 0.2–0.3 and 40–60%, respectively.

$$BI = \frac{YM\_BRIT + PR\_BRIT}{2} \tag{4}$$

$$YM_{\mathrm{BRIT}} = \frac{YMSC - YM_{\min}}{YM_{max} - YM_{\min}} \times 100\% \tag{5}$$

$$PR_{\mathrm{BRIT}} = \frac{PRC - PR_{\max}}{PR_{\min} - PR_{\max}} \times 100\% \tag{6}$$

where YMSC refers to Young's modulus (10^4 MPa); PRC is Poisson's ratio (dimensionless); YM_BRIT is Young's modulus after normalization (dimensionless); PR_BRIT is Poisson's ratio after normalization (dimensionless); BI refers to the brittleness index; and YMmax, YMmin, PRmin and PRmax are the maximum and minimum values of Young's modulus and Poisson's ratio, respectively.

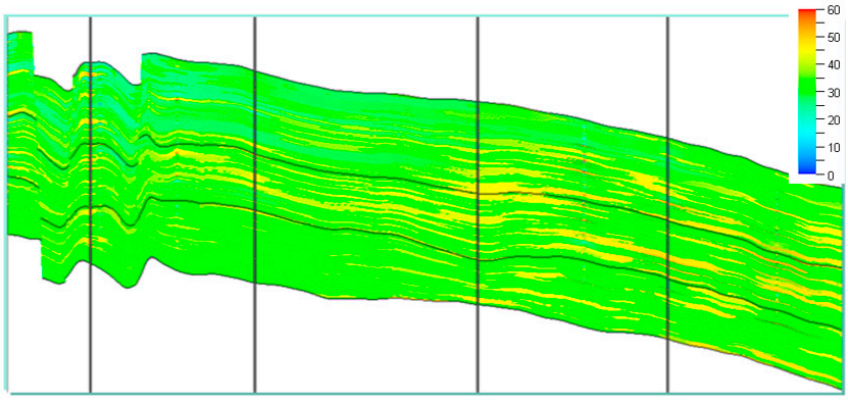

Figure 8. Cross-section map of Young's modulus in the N–S direction.

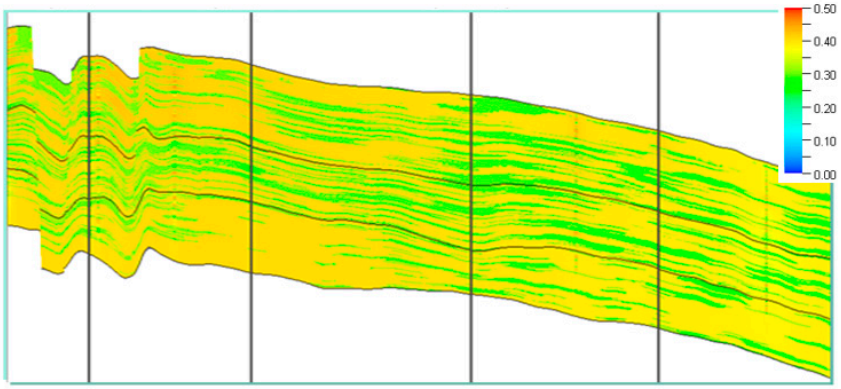

Figure 9. Cross-section map of Poisson ratio in the N–S direction.

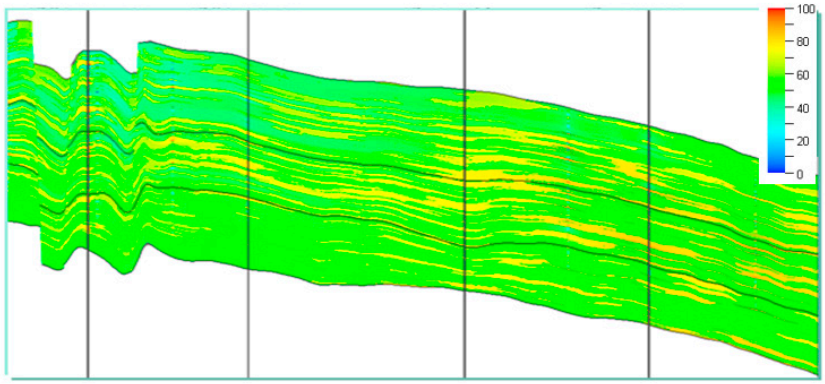

Figure 10. Cross-section map of the brittleness index in the N–S direction.

Based on the geomechanical modeling results, the geomechanical parameters were calibrated by history matching of an existing well fracturing operation with the production history so as to ensure the precision of the simulation model. Figure 11 shows the production history matching result, which is in agreement with the actual field operations. Figure 12 shows the spatial fracture distribution in each payzone, which indicates that the fractures are highly affected by the reservoir heterogeneity and stress changes in each zone.

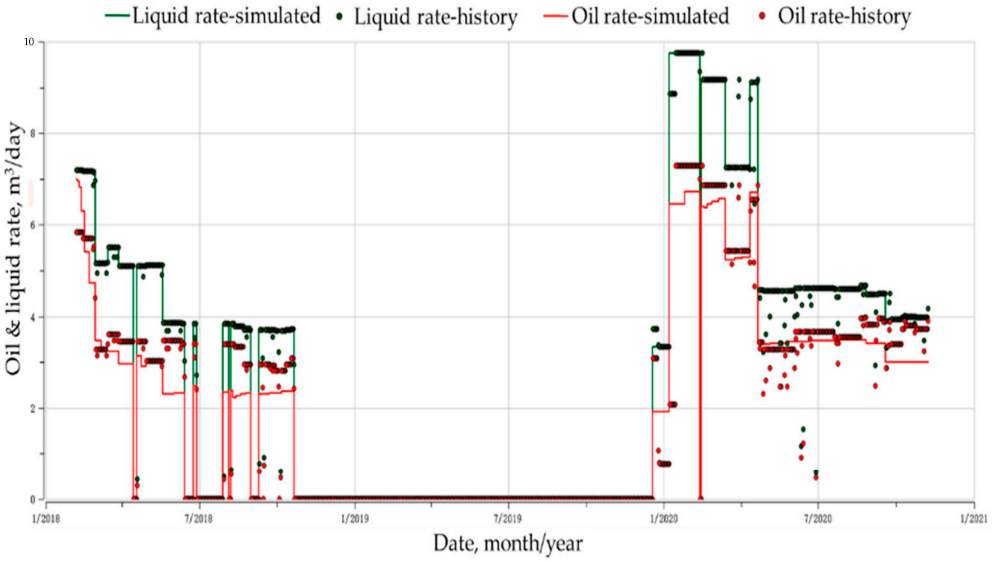

Figure 11. History matching curves of the liquid rate and oil rate.

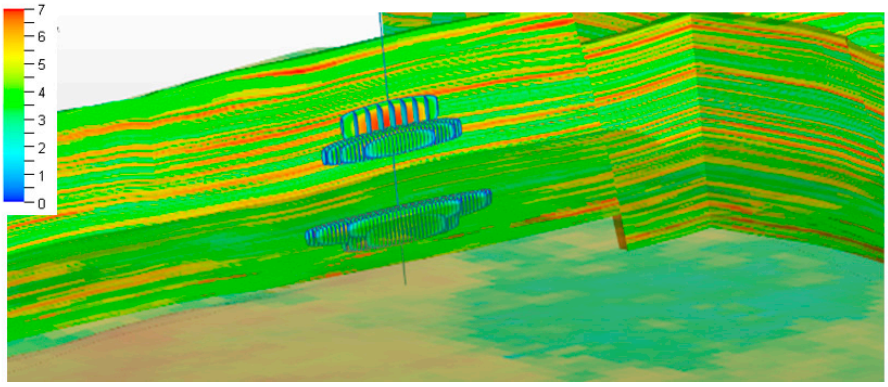

Figure 12. Spatial distribution of fractures under heterogeneous conditions.

The petrophysical and geomechanical parameters of each layer in the work area were calibrated by history matching, providing a data reference for subsequent sensitivity analysis of fracturing and reservoir parameter simulation. A comparison of the results obtained using the traditional method and those obtained using the method proposed in this study based on the statistics before and after history matching is shown in Table 1, which indicates an obvious variance, as reflected in the second column showing traditional calculation results. History matching using existing fracturing and production data is critical to further calibrate the geomechanical parameters, particularly in multilayer reservoirs.

Table 1. Comparison of geomechanical parameters before and after calibration.

Item	Traditional Calculation	Before History Matching	After History Matching
Minimum horizontal principal stress	22–30 MPa	25–32 MPa	24.6–30.7 MPa
Reservoir stress difference between payzone and interlayer	1.1–9.1 MPa	2–10 MPa	0.5–2.5 MPa
Young's modulus	15.6–25.1 GPa	15–27 GPa	16.1–29.2 GPa
Poisson's ratio	0.22–0.35	0.2–0.3	0.25–0.34

4. Influence Factors on Volumetric Fracturing Performance

4.1. Numerical Simulation Model Coupled with Rock Geomechanics

Figure 13 shows the heterogeneous numerical simulation model properties. Using the geomechanical parameters and the reservoir heterogeneous properties, a 6X numerical simulator was chosen to build a typical heterogeneous well model to investigate the influencing factors, including both reservoir properties and geomechanical factors.

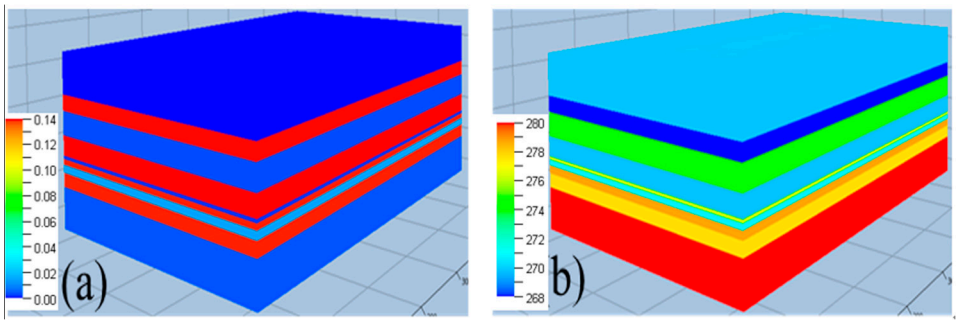

Figure 13. Heterogeneous numerical simulation model properties. (**a**) Porosity model; (**b**) minimum horizontal principal stress model.

According to the calibrated geological and in situ stress parameters of the study area, a coupling numerical simulation mechanism model of a reservoir and fracture system was established, in which the influence of formation longitudinal heterogeneity and well and

fracturing parameter changes on fracturing effect is simulated, and the sensitive factors of fracturing effect in the study area are determined. The values of key properties in the sensitivity model are listed in Table 2.

Table 2. Spatial distribution of fractures under heterogeneous conditions.

Category	Item	Level 1	Level 2	Level 3	Level 4	Level 5
Geological and geomechanical parameters	Payzone thickness (m)	2	3	4	5	6
	Permeability (mD)	0.2	0.5	0.8	1.2	1.5
	Interlayer thickness (m)	6	8	10	12	14
	Stress difference between payzone and interlayer (MPa)	0.5	1	1.5	2	2.5
	Poisson's ratio	0.2	0.25	0.3	0.35	/
	Young's modulus (GPa)	15	20	25	30	/
Fracturing parameters	Injection rate (m^3/min)	4	6	8	10	12
	Liquid intensity (m^3/m)	250	300	350	400	450
	Sand intensity (m^3/m)	16	18	20	22	24
	Fracturing spacing (m)	5	10	15	20	25

Based on the calibrated model presented in Section 3, the influence of reservoir payzone thickness, formation permeability, interlayer thickness, stress difference between payzone and interlayer, Young's modulus and Poisson's ratio on post-fracturing production was studied by mechanism numerical simulation, and the production performance curve was analyzed to determine the effect of sensitive factors.

4.2. Influence of Geological and Geomechanical Parameters on Volumetric Fracturing

(1) Payzone thickness

Figure 14a shows the permeability distribution after fracturing, and Figure 14b shows the permeability distribution after 6 years of production. Based on a comparison of simulation results, vertical well volumetric fracturing and production were simulated under payzone thicknesses of 2 m, 3 m, 4 m and 5 m. The simulation results show that with an increase in reservoir payzone thickness, the length/width ratio of the fracture network increases. The fracture length ranges from 145 m to 170 m, and the maximum fracture-effected width is 50 m. When the payzone thickness is 5 m, there is a significant change in fracture dimensions compared with other fractures. A comparison of fracture permeability shows that as production continues, the fracture gradually closes.

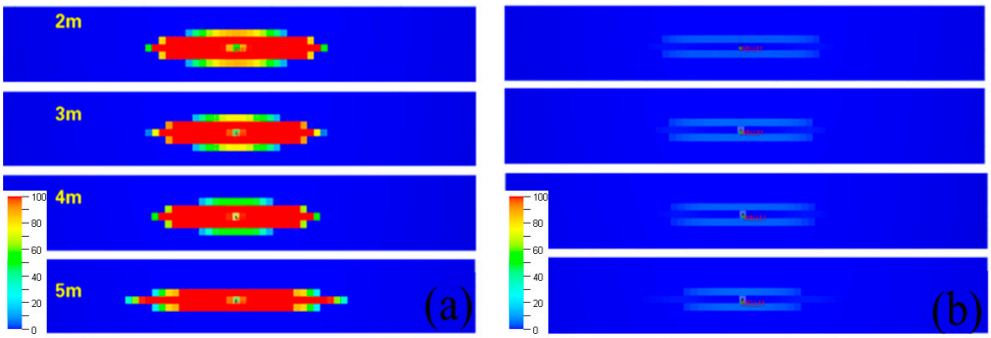

Figure 14. Planar fracture permeability distribution with different payzone thickness values. (**a**) After fracturing; (**b**) after 6 years of production.

Figure 15 shows that the oil saturation distribution is basically consistent with the fracture network configuration at the end of fracturing. As production continues, the range of reservoir production expands relative to the fractured volume. After 6 years of

production, the plane length and width of the oil drainage area range from 310 m to 370 m and from 50 m to 70 m, respectively.

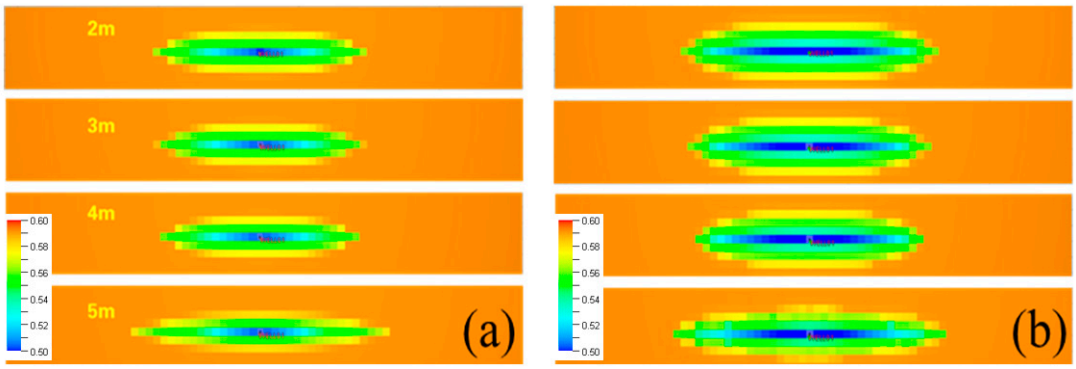

Figure 15. Planar oil saturation distribution with different payzone thickness values. (**a**) After fracturing; (**b**) after 6 years of production.

As indicted by the perspectives of production effect shown in Figure 16, the cumulative production increases with payzone thickness, and accumulative oil production varies greatly with different reservoir thicknesses. The cumulative oil production after 3 and 6 years with a reservoir thickness of 5 m is 324.71 m^3 and 394.74 m^3 higher, respectively, than with a reservoir thickness of 2 m because the condition of the reservoir itself is the material basis for the size of tight oil reserves and the productivity of a single well. Therefore, the development scale and reservoir geological characteristics of a "sweet spot" should be carefully considered when designing fracturing schemes.

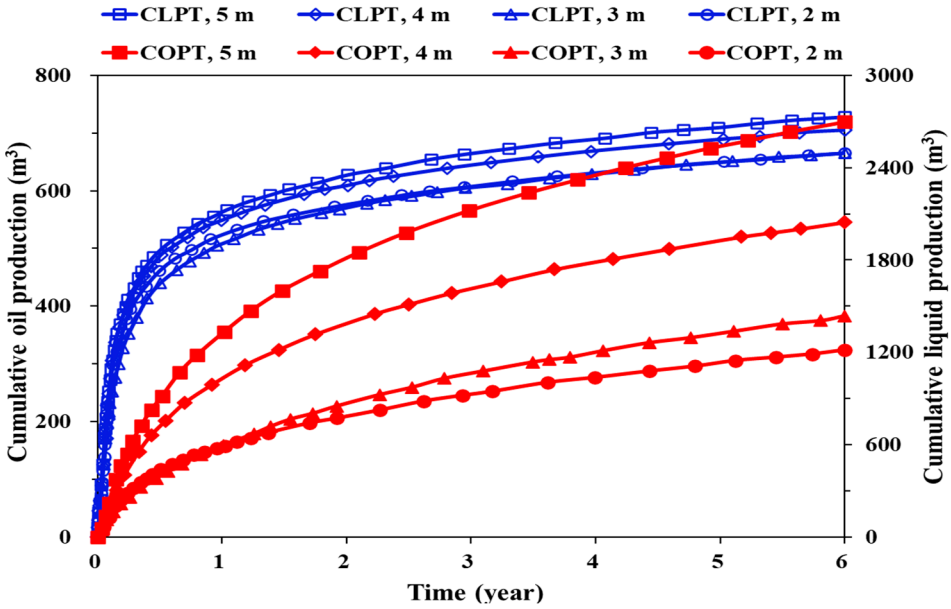

Figure 16. Production performance curves of different payzone thickness values (6 years of production).

(2) Formation permeability

Based on the production effect comparison shown in Figure 17, the liquid production remains almost the same when the formation permeability changes from 0.5 mD to 2.5 mD because the flow capacity is mostly correlated with the fractured performance under such permeability levels but is less impacted by the initial formation permeability.

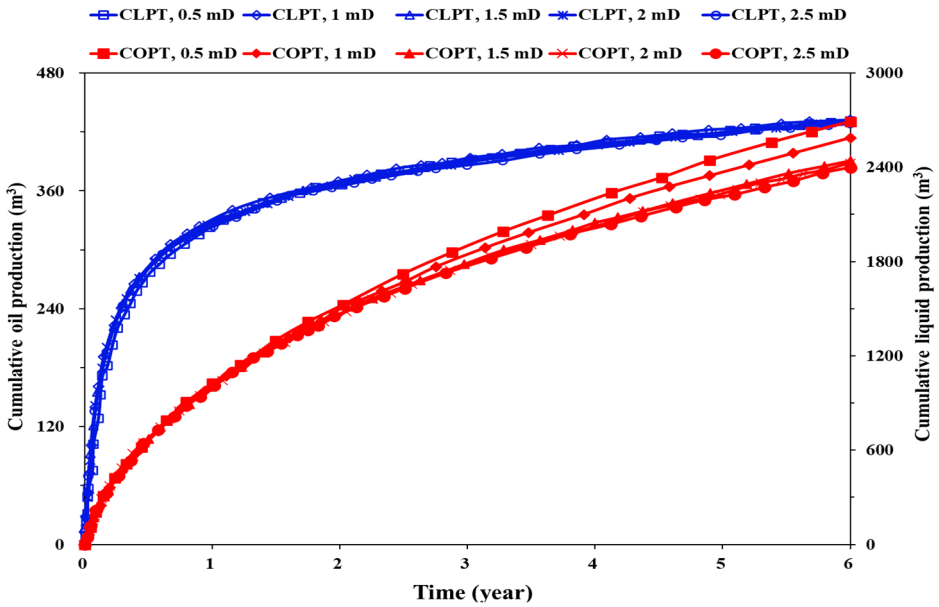

Figure 17. Production performance curves with different formation permeability values (6 years of production).

In contrast, the oil production increases with a decrease in formation permeability, but the range of change is relatively small because the initial formation permeability has little influence on the fractured volume, which is mostly controlled by fracturing operations.

(3) Interlayer thickness

Figure 18 shows that accumulative liquid production and accumulative oil production increase with increased interlayer thickness, and accumulative oil production varies greatly with different interlayer thicknesses. Cumulative oil production after 3 and 6 years with an interlayer thickness of 14 m is 357.32 m^3 and 371.70 m^3 higher, respectively, than with an interlayer thickness of 6 m because the longitudinal fracture height is strongly affected by interlayer thickness.

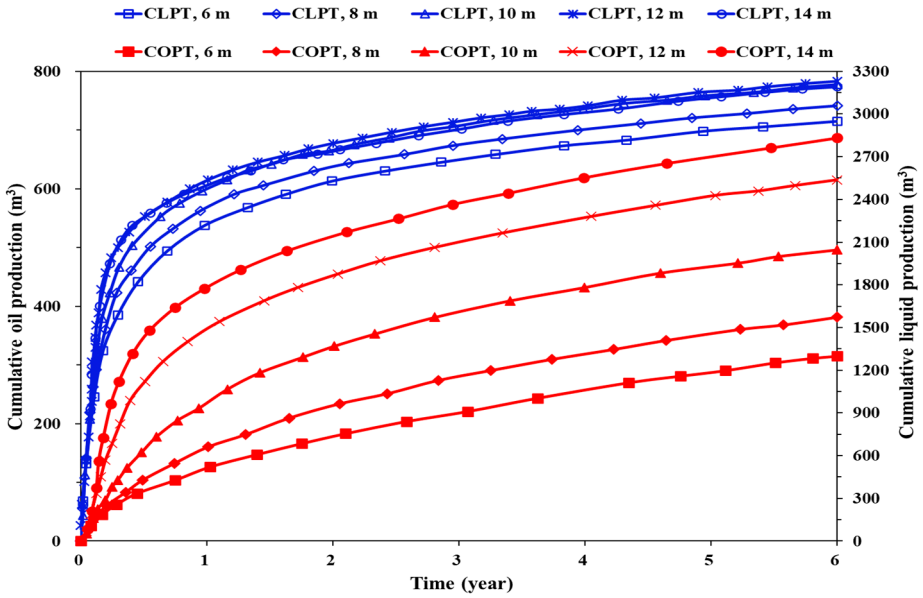

Figure 18. Production performance curves with different interlayer thickness values (6 years of production).

(4) Stress difference of the payzone and interlayer

Figure 19a shows the permeability distribution after fracturing, and Figure 19b shows the permeability distribution after 6 years of production. The simulation results show that with an increase in stress difference, the length and bandwidth of the target layer exhibit an increasing trend. The distribution range is 165–195 m, and the maximum bandwidth is 30 m, expanding along the direction of the seam length. As production progresses, the fractures gradually close, and the smaller the stress difference, the faster the closure, which is positively correlated with the degree of deficit.

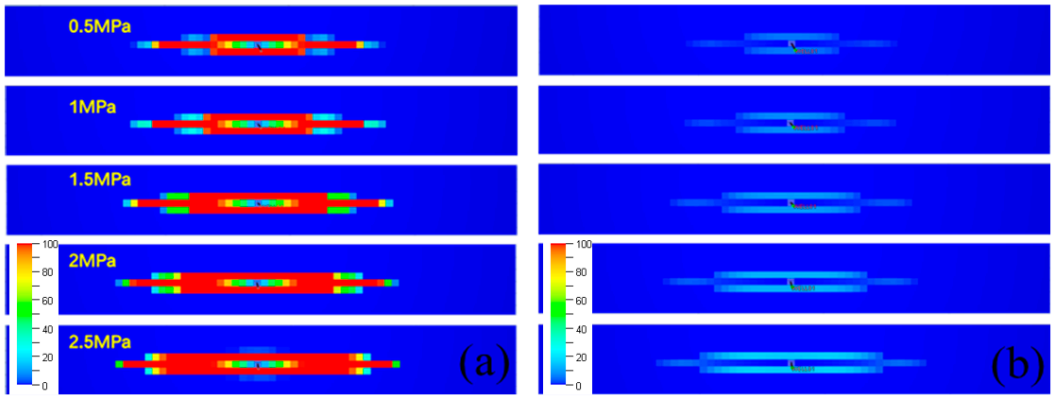

Figure 19. Planar fracture permeability distribution with varying stress difference. (**a**) After fracturing; (**b**) after 6 years of production.

As shown in Figure 20, accumulative liquid production and accumulative oil production increase with the stress difference between the reservoir and interlayer. The cumulative incremental oil production after 3 and 6 years with a stress difference of 2.5 MPa is 101.98 m^3 and 137.14 m^3 higher than the case with a stress difference of 0.5 MPa. Therefore, higher reservoir stress difference is more conducive to achieving effective reservoir fracturing and better production effect.

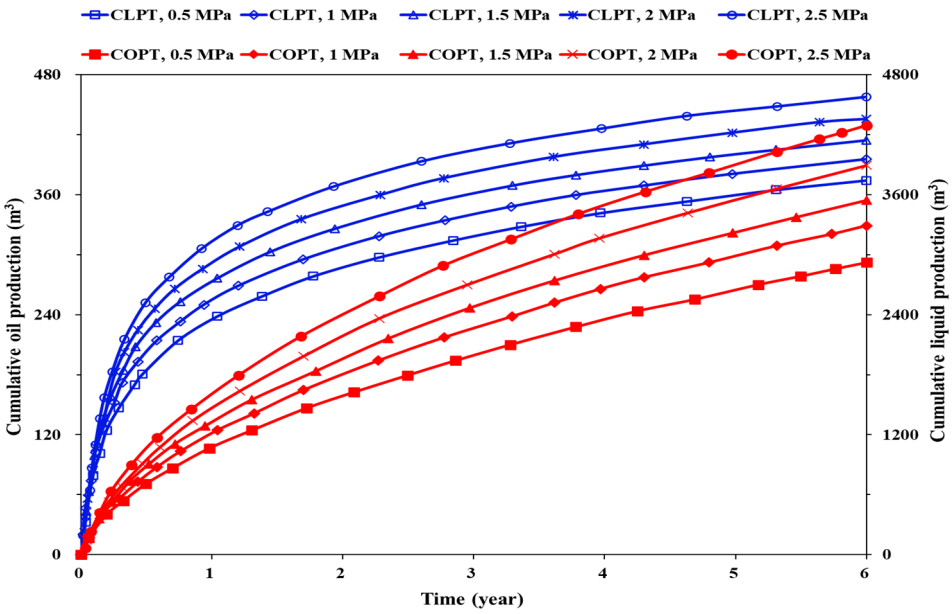

Figure 20. Production performance curves with varying stress difference (6 years of production).

(5) Young's modulus

Figure 21 shows the oil production performance curves for different Young's modulus values. From the perspective of production effect, accumulative liquid production and

accumulative oil production are basically the same, so Young's modulus is not considered a sensitive factor.

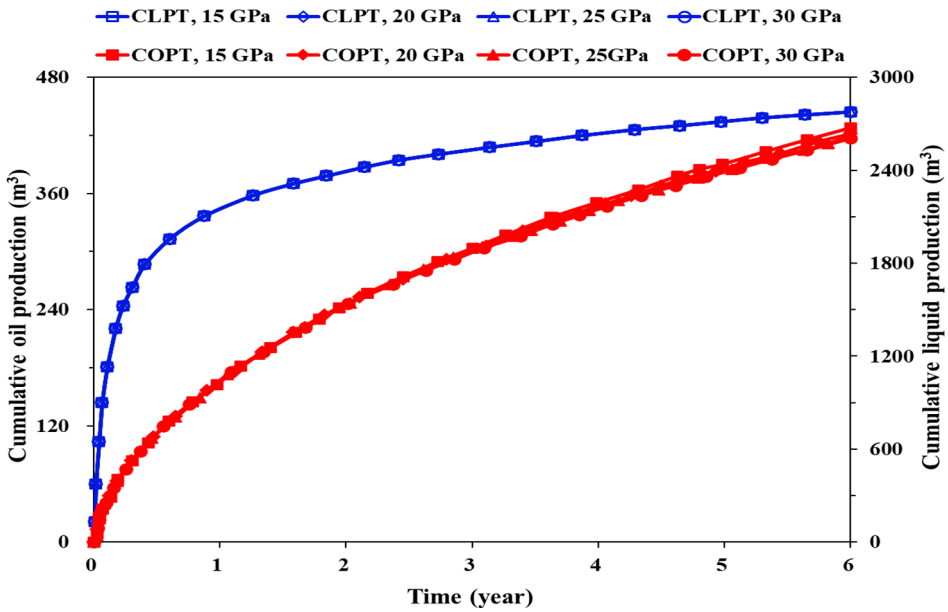

Figure 21. Production performance curves for different Young's modulus values.

(6) Poisson's ratio

Figure 22 indicates that the liquid production is the same when the Poisson's ratio varies from 0.2 to 0.35, but the oil production increases with a decrease in Poisson's ratio, whereas the overall difference is not significant.

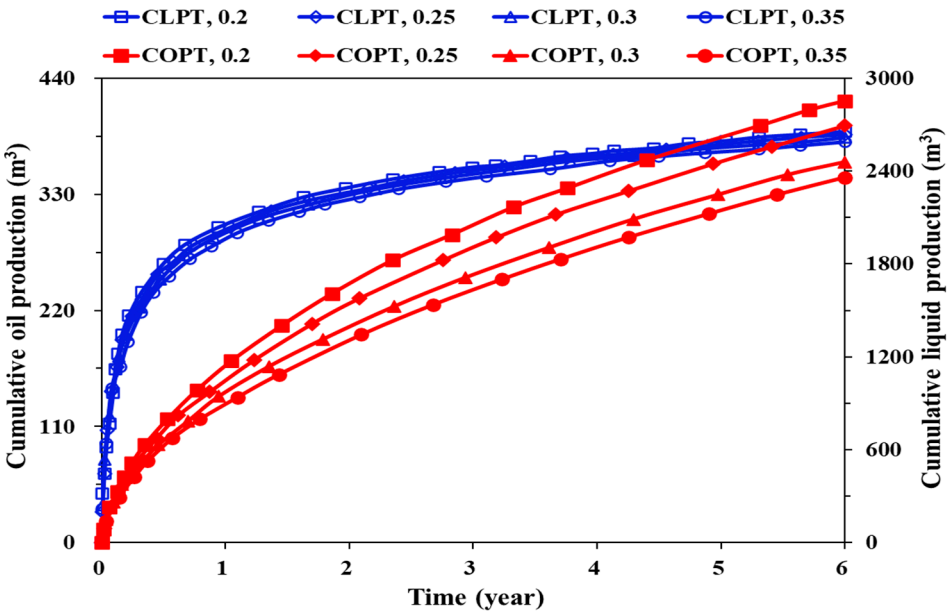

Figure 22. Production performance curves for different Poisson's ratio values.

4.3. Influence of Fracturing Parameters on Volumetric Fracturing

The mechanism numerical model is used to study the influence of injection rate, liquid intensity, sand intensity and fracturing spacing of horizontal wells on the oil production effect after fracturing, analyze the productivity change curve and determine the sensitive factors. Figures 23 and 24 show that the variation of each fracturing parameter is sensitive to the productivity. Oil production increases with increases in construction displacement,

liquid volume and sand volume and increases with decreased fracture spacing of horizontal wells. The oil production changes with changes in the liquid injection rate and liquid volume, whereas with changes in sand volume and fracture spacing of horizontal wells, the oil production varies significantly.

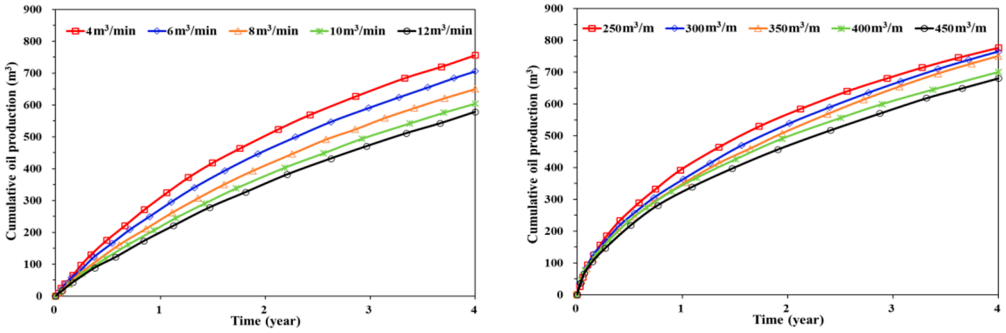

Figure 23. Injection rate and liquid injection intensity sensitivity.

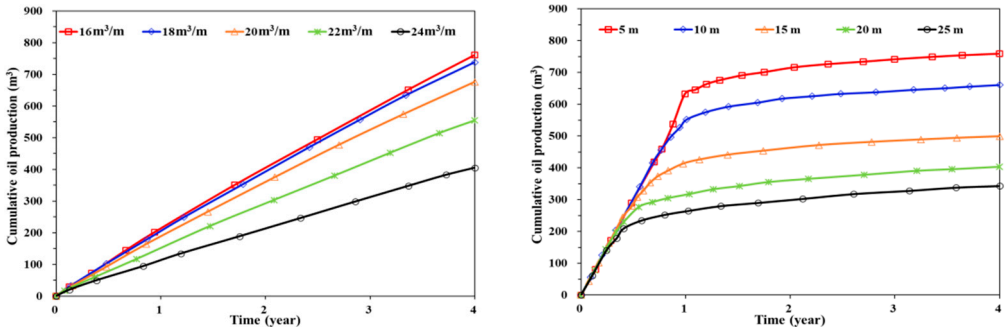

Figure 24. Sand volume intensity and fracturing spacing sensitivity.

5. Pilot Well Design and Oil Production Performance

The pilot well was placed in the WTG formation group in Xinjiang Oilfield, which is yet to be exploited due to the ultra-low permeability in this tight oil reservoir. The evolution of hydraulic volumetric fracturing technology makes it possible to realize commercialized development through careful fracturing design. The success of the pilot well is of great significance to the development of this area, so the methodology proposed in this study was used to guide the fracturing design.

Using the workflow proposed in this study, the typical pilot well in this area was chosen, and geomechanical modeling was performed based on the petrophysical properties. Figure 25 displays the 3D porosity and minimum principal stress modeling results. The grid dimensions are 20 m × 10 m × 0.2–1 m, and the total grid number is 328,891.

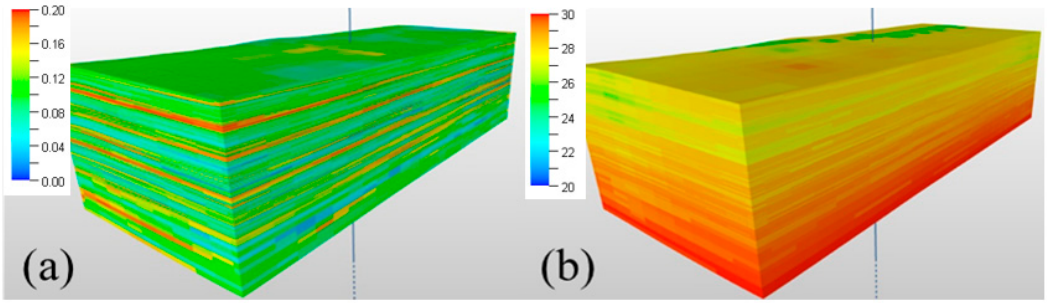

Figure 25. Three-dimensional porosity and minimum principal stress modeling results. (**a**) Porosity; (**b**) minimum principal stress.

Based on the geomechanical model, the hydraulic fracturing parameters were designed, and the production performance was forecasted; the hydraulic fracturing design results for each zone are listed in Table 3.

Table 3. Results of the pilot well after hydraulic fracturing design optimization.

Zone No.	Slickwater m^3	Water m^3	Preflush m^3	Sand-Carrying Fluid m^3	Displacement Fluid m^3	Total Liquid m^3	100 Mesh m^3	40–70 Mesh m^3	20–40 Mesh m^3	Total Sand
1#	405	135	16	75.7	7.3	639	3	17	3	23
2#	1480	490	50	265.6	7.8	2293.4	9	69	5	83
3#	2350	750	100	563.1	7.7	3770.8	14	113	8	135
4#	1740	560	60	330.9	7.7	2698.6	11	84	5	100
5#	795	265	28	152.2	7.5	1247.7	5	35	5	45
6#	1125	375	36	199.6	7.4	1743	7	50	5	62
7#	855	285	28	152	7.3	1327.3	5	38	5	48

Figure 26 shows the fracture evolution after fracturing, and Figure 27 displays the horizontal permeability changes after fracturing and after two years of production. Based on the simulation results, the main fracture length is 223–341 m, the length of the branch fractures is 146–234 m and the fractured volume is 1.85 × 106 m^3. The overall permeability after fracturing is 535 mD, and it gradually declines to 260 mD after production for two years, which is still much higher than that before fracturing.

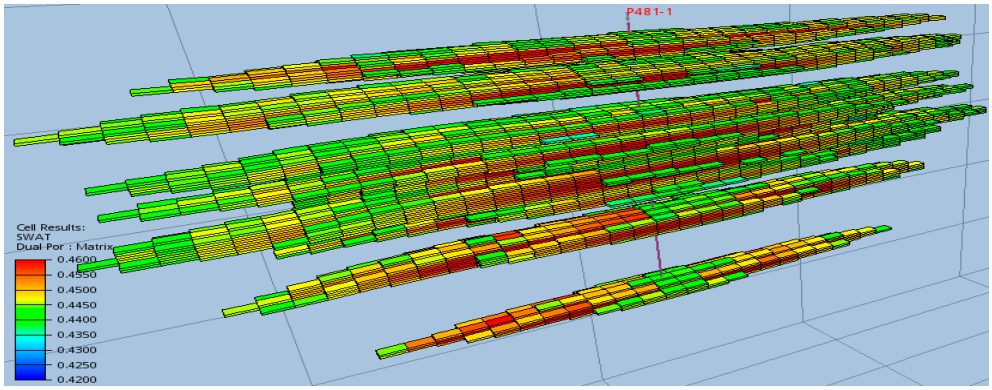

Figure 26. Fracture evolution after fracturing.

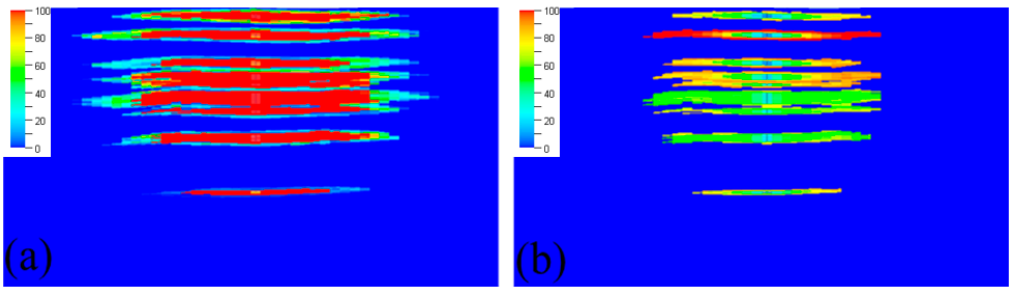

Figure 27. Horizontal permeability changes over time. (**a**) After fracturing; (**b**) after two years of production.

As shown in Figure 28, the production performance of the optimized fracturing pilot well was predicted and compared with that of the adjacent well, which was treated by traditional commingle hydraulic fracturing. It is obvious that the highest oil rate of the pilot well is 12 tons/day, which is enhanced by 7 tons/day relative to traditional fracturing. Furthermore, the oil rate declination rate is also quite different. After one year

of production, the oil rate remains at 6.3 tons/day, whereas that of traditional fracturing reaches the economic limit of production (2.5 tons/day). It is predicted that the total incremental oil of the first year could reach 2030 tons.

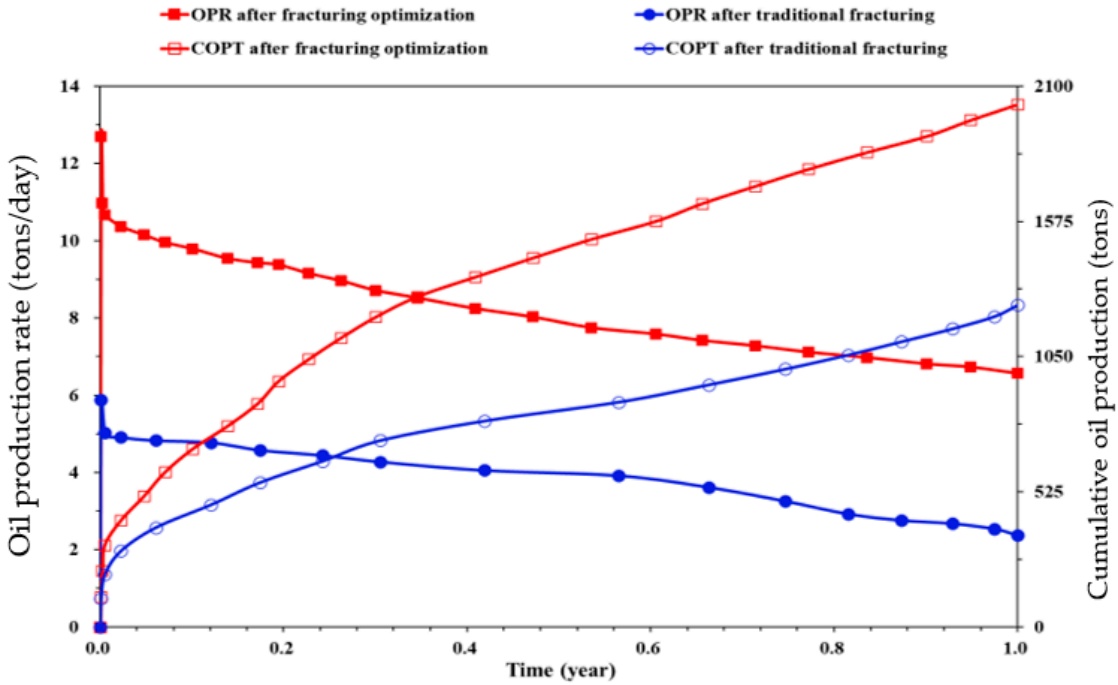

Figure 28. Productivity comparison of the pilot well after tradition fracturing and after optimized fracturing.

6. Conclusions

(1) A workflow of a 3D fine geomechanical model was proposed, including a structure model, petrophysical model and geomechanical model. The geomechanical model parameters of a typical reservoir were comprehensively corrected through production history matching.

(2) The sensitive factors affecting fracturing production in this area were evaluated numerically. The influence of formation parameters and operational parameters on volume fracturing was studied with oil production as the main index. The results show that for formation parameters, the payzone thickness of the reservoir is the main influencing factor; the interlayer thickness and stress difference between the reservoir and interlayer are the secondary influencing factors; and the formation permeability, Young's modulus and Poisson's ratio are the weak influencing factors.

(3) A typical pilot test well was designed, fracturing parameters were optimized and the production before and after optimized fracturing was predicted and compared. The results show that optimized fracturing can increase the oil production rate by 7 tons/day relative to traditional fracturing. The oil production rate is 4 tons/day higher than that of conventional fracturing after 1 year of production, indicating encouraging incremental performance.

Author Contributions: D.D. designed and conducted the experiments and wrote the main manuscript text; Y.W. conducted numerical simulation; X.X. revised the main manuscript text; W.L. designed the experiment; J.Z. and P.L. prepared all of the figures. All authors have read and agreed to the published version of the manuscript.

Funding: This research was funded by the China National Key Project (2016ZX05031) and the Science and Technology Project of CNPC (2021DJ3208 and 2021DJ1403).

Institutional Review Board Statement: Not applicable.

Informed Consent Statement: Not applicable.

Data Availability Statement: Not applicable.

Conflicts of Interest: The authors declare no conflict of interest.

References

1. Alexeyev, A.; Ostadhassan, M.; Mohammed, R.A.; Bubach, B.; Khatibi, S.; Li, C.; Kong, L. Well log based geomechanical and petrophysical analysis of the bakken formation. In Proceedings of the 51st US Rock Mechanics/Geomechanics Symposium, OnePetro, San Francisco, CA, USA, 25–28 June 2017.
2. Eshkalak, M.O.; Mohaghegh, S.D.; Esmaili, S. Geomechanical properties of unconventional shale reservoirs. *J. Pet. Eng.* **2014**, *2014*, 1–10. [CrossRef]
3. Zoccarato, C.; Baù, D.; Bottazzi, F.; Ferronato, M.; Gambolati, G.; Mantica, S.; Teatini, P. On the importance of the heterogeneity assumption in the characterization of reservoir geomechanical properties. *Geophys. J. Int.* **2018**, *207*, 47–58. [CrossRef]
4. Mallet, C.; Isch, A.; Laurent, G.; Jodry, C.; Azaroual, M. Integrated static and dynamic geophysical and geomechanical data for characterization of transport properties. *Int. J. Rock Mech. Min. Sci.* **2022**, *153*, 105050. [CrossRef]
5. Vishkai, M.; Wang, J.; Wong, R.C.; Clarkson, C.R.; Gates, I.D. Modeling geomechanical properties in the montney formation, Alberta, Canada. *Int. J. Rock Mech. Min. Sci.* **2017**, *96*, 94–105. [CrossRef]
6. Germay, C.; Richard, T.; Mappanyompa, E.; Lindsay, C.; Kitching, D.; Khaksar, A. The continuous-scratch profile: A high-resolution strength log for geomechanical and petrophysical characterization of rocks. *SPE Reserv. Eval. Eng.* **2015**, *18*, 432–440. [CrossRef]
7. Schön, J.H. Geomechanical properties. In *Developments in Petroleum Science*; Elsevier: Amsterdam, The Netherlands, 2015; Volume 65, pp. 269–300.
8. Zhao, Z.; Kai, L.I.; Zhao, P.; Tao, L. Practice and development suggestions for volumetric fracturing technology for shale oil in the ordos basin. *Pet. Drill. Tech.* **2021**, *49*, 85–91.
9. Chen, Y.; Zhang, D. Well log generation via ensemble long short-term memory (EnLSTM) network. *Geophys. Res. Lett.* **2020**, *47*, e2020GL087685. [CrossRef]
10. Tahmeen, M.; Love, J.; Rashidi, B.; Hareland, G. Complete geomechanical property log from drilling data in unconventional horizontal wells. In Proceedings of the 51st US Rock Mechanics/Geomechanics Symposium, OnePetro, San Francisco, CA, USA, 25–28 June 2017.
11. Carpenter, C. Surface drilling data can help optimize fracture treatment in real time. *J. Pet. Technol.* **2019**, *71*, 74–76. [CrossRef]
12. Elkatatny, S.; Tariq, Z.; Mahmoud, M.; Mohamed, I.; Abdulraheem, A. Development of new mathematical model for compressional and shear sonic times from wireline log data using artificial intelligence neural networks (white box). *Arab. J. Sci. Eng.* **2018**, *43*, 6375–6389. [CrossRef]
13. Parapuram, G.; Mokhtari, M.; Ben Hmida, J. An artificially intelligent technique to generate synthetic geomechanical well logs for the bakken formation. *Energies* **2018**, *11*, 680. [CrossRef]
14. Parapuram, G.K.; Mokhtari, M.; Hmida, J.B. Prediction and analysis of geomechanical properties of the upper bakken shale utilizing artificial intelligence and data mining. In Proceedings of the SPE/AAPG/SEG Unconventional Resources Technology Conference, OnePetro, Austin, TX, USA, 24–26 July 2017.
15. Akinnikawe, O.; Lyne, S.; Roberts, J. Synthetic well log generation using machine learning techniques. In Proceedings of the SPE/AAPG/SEG Unconventional Resources Technology Conference, OnePetro, Houston, TX, USA, 23–25 July 2018.
16. Chen, Y.; Zhang, D. Physics-constrained deep learning of geomechanical logs. *IEEE Trans. Geosci. Remote Sens.* **2020**, *58*, 5932–5943. [CrossRef]
17. Miah, M.I. Predictive models and feature ranking in reservoir geomechanics: A critical review and research guidelines. *J. Nat. Gas Sci. Eng.* **2020**, *82*, 103493. [CrossRef]
18. Farquhar, R.A.; Somerville, J.M.; Smart, B.G.D. Porosity as a geomechanical indicator: An application of core and log data and rock mechanics. In Proceedings of the European Petroleum Conference, OnePetro, London, UK, 25–27 October 1994.
19. Slatt, R.M.; Abousleiman, Y. Merging sequence stratigraphy and geomechanics for unconventional gas shales. *Lead. Edge* **2011**, *30*, 274–282. [CrossRef]
20. Grana, D.; Schlanser, K.; Campbell-Stone, E. Petroelastic and geomechanical classification of lithologic facies in the Marcellus Shale. *Interpretation* **2015**, *3*, SA51–SA63. [CrossRef]
21. Gray, D.; Anderson, P.; Logel, J.; Delbecq, F.; Schmidt, D.; Schmid, R. Estimation of stress and geomechanical properties using 3D seismic data. *First Break* **2012**, *30*, 59–68. [CrossRef]
22. Hussain, M.; Ahmed, N. Reservoir geomechanics parameters estimation using well logs and seismic reflection data: Insight from Sinjhoro Field, Lower Indus Basin, Pakistan. *Arab. J. Sci. Eng.* **2018**, *43*, 3699–3715. [CrossRef]
23. Matinkia, M.; Amraeiniya, A.; Behboud, M.M.; Mehrad, M.; Bajolvand, M.; Gandomgoun, M.H.; Gandomgoun, M. A novel approach to pore pressure modeling based on conventional well logs using convolutional neural network. *J. Pet. Sci. Eng.* **2022**, *211*, 110156. [CrossRef]

24. Liu, Z.; Song, L.; Wang, C.; Sun, T.; Yang, X.; Xia, L.I. Evaluation method of the least horizontal principal stress by logging data in anisotropic fast formations. *Pet. Explor. Dev.* **2017**, *44*, 789–796. [CrossRef]
25. Tan, W.H.; Ba, J.; Guo, M.Q.; Li, H.; Zhang, L.; Yu, T.; Chen, H. Brittleness characteristics of tight oil siltstones. *Appl. Geophys.* **2018**, *15*, 14. [CrossRef]